

Attentional Graph Neural Networks for Robust Massive Network Localization

Wenzhong Yan, Juntao Wang, Feng Yin, *Senior Member, IEEE*, and Abdelhak M. Zoubir, *Fellow, IEEE*

Abstract—Graph neural networks (GNNs) have gained significant popularity for classification tasks in machine learning, yet their applications to regression problems remain limited. Concurrently, attention mechanisms have emerged as powerful tools in sequential learning tasks. In this paper, we employ GNNs and attention mechanisms to address a classical but challenging nonlinear regression problem: network localization. We propose a novel GNN-based network localization method that achieves exceptional stability and accuracy in the presence of severe non-line-of-sight (NLOS) propagations, while eliminating the need for laborious offline calibration or NLOS identification. Extensive experimental results validate the effectiveness and high accuracy of our GNN-based localization model, particularly in challenging NLOS scenarios. However, the proposed GNN-based model exhibits limited flexibility, and its accuracy is highly sensitive to a specific hyperparameter that determines the graph structure. To address the limitations and extend the applicability of the GNN-based model to real scenarios, we introduce two attentional graph neural networks (AGNNs) that offer enhanced flexibility and the ability to automatically learn the optimal hyperparameter for each node. Experimental results confirm that the AGNN models are able to enhance localization accuracy, providing a promising solution for real-world applications. We also provide some analyses of the improved performance achieved by the AGNN models from the perspectives of dynamic attention and signal denoising characteristics.

Index Terms—Graph neural networks, non-line-of-sight, massive network localization, attention mechanism, distributed learning.

I. INTRODUCTION

In recent years, graph neural networks (GNNs) have achieved many state-of-the-art results in various graph-related learning tasks such as node classification, link prediction and graph classification [1]–[4]. Comparing with the multi-layer perceptrons (MLPs), GNNs can exploit extra information about edges. More concretely, each node aggregates information of its adjacent nodes instead of just using its own [5], [6]. Though being effective, GNN models are often used to deal with classification tasks with discrete labels. While regression problems are more challenging and constitute a large body of practical signal processing applications.

Additionally, attention mechanisms have recently achieved great success in many sequential learning tasks [7], [8]. The underlying principle is to learn a function that aggregates a variable-sized input while focusing on the parts relevant to a given context. When a single sequence is used as both the input and context, it is called self-attention. Though attention mechanisms were initially designed to facilitate RNNs to capture long-range dependencies, Vaswani et al. [9] demonstrates the efficacy of a pure self-attention network in achieving state-of-the-art performance in machine translation, while being significantly more efficient.

In this paper, we consider a classic yet challenging nonlinear regression problem, namely large-scale network localization. Network localization requires not only the measurements between agent nodes and anchor nodes, but also the measurements between the agent nodes themselves. In the past decades, a variety of canonical network localization methods have been developed, including 1) maximum likelihood estimation based methods [10]–[13]; 2) least-squares estimation based methods [14]; 3) multi-dimensional scaling based methods [15]; 4) mathematical programming based methods [16], [17] and 5) Bayesian message passing based methods [18], [19].

Ignoring the effect due to non-line-of-sight (NLOS) propagation will incur severe performance degradation of the aforementioned methods. For remedy, the most applied strategy is to perform NLOS identification for each link and then either discard the NLOS measurements or suppress them in the aforementioned methods [20]. However, accurate NLOS identification requires large-scale offline calibration and huge manpower. The NLOS effect can also be dealt with from algorithmic aspect. Based on the assumption that NLOS noise follows a certain probability distribution, the maximum likelihood estimation based methods were developed in [21], [22]. However, model mismatch may cause severe performance degradation. In a recent work [23], [24], network localization problem is formulated as a regularized optimization problem in which the NLOS-inducing sparsity of the ranging-bias parameters was exploited. Unfortunately, all of these methods are computationally expensive for massive networks.

Taking all these factors into account, in this paper,

we propose fresh GNN-based network localization method. Experimental results show that the GNN-based localization model provides extremely stable and highly accurate localization accuracy despite severe NLOS propagations. Besides, it does not require laborious offline calibration or NLOS identification. As far as we know, this is the first time that GNN has been applied to network localization. However, the localization accuracy of the proposed GNN-based model is sensitive to a hyperparameter that determines the graph structure, and its optimal value would change as the node moves. To extend the GNN based model to a realistic scenario, two attentional graph neural network (AGNN) models are proposed to automatically learn the optimal hyperparameter for each node. Additionally, we provide some fundamental analyses for the improved performance of the proposed AGNN models from the perspective of dynamic attention and signal denoising characteristics.

Lastly, we would like to mention that this paper is an extension of our previous work, [25], in which only the GCN-based network localization method (see Sec. III-A) was considered.

The remainder of this paper is organized as follows. The background of network localization and problem formulation are introduced in Sec. II. In Sec. III-A, we introduce a fresh GCN framework for network localization. To extend to a general scenario, two AGNN models are proposed in Sec. IV. Finally, we conclude the paper in Section VII.

Notation: Boldface lowercase letter \mathbf{x} and boldface uppercase letter \mathbf{X} are conventionally used to signify vectors and matrices, respectively. \mathbf{x}_i and $\mathbf{x}_{[i,:]}$ designate the i -th column and row of matrix \mathbf{X} , respectively. Meanwhile, the element in the i -th row and j -th column of matrix \mathbf{X} is denoted by x_{ij} . The calligraphic letter \mathcal{N} is conventionally employed to denote a set, where $|\mathcal{N}|$ signifies the cardinality of this set. $[N]$ denotes the represents the set of natural numbers from 1 to N . The operator $(\cdot)^\top$ signifies vector/matrix transpose. $\|\cdot\|$ represents the Euclidean norm of a vector. $\|\cdot\|_F$ denotes the Frobenius norm of a matrix. $[\cdot|\cdot]$ stands for the column/row concatenation operation for two column/row vectors. $\mathbf{X} \odot \mathbf{Y}$ represents the Hadamard product of two matrices with identical dimensions.

II. LOCALIZATION SCENARIO AND PROBLEM FORMULATION

A. Localization Scenario

The depicted scenario in Fig. 1 illustrates a network localization setup. In the context of a massive wireless network, a limited number of nodes, known as anchors, possess precise location information obtained through GPS/BeiDou chips. Conversely, the remaining nodes, referred to agents, lack access to GPS, and consequently they need to be located. Equipped with omni-directional antennas, each node broadcasts signals containing information, such as node ID,

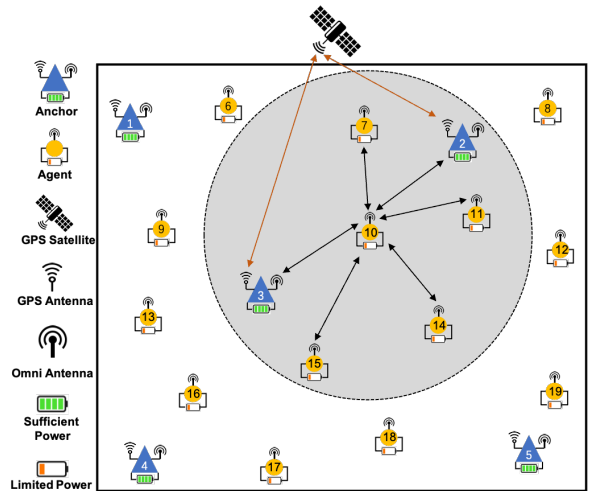


Fig. 1: Network localization scenario.

transmit power, transmit time, as well as network configurations.

This scenario well suits many realistic massive wireless networks. For instance, in 5G network, a substantial number of small base stations are densely deployed within each cell. Similarly, in the Internet of Things (IoT) network, which advocates the interconnection of a wide array of devices and machines [26], comprises a substantial number of interconnected smart devices. For massive networks, it is common that only a small fraction of nodes possess their precise locations. To determine the locations of all nodes, otherwise, significant human resources would be required for offline calibration, or alternatively, the installation of costly and power-intensive GPS/BeiDou chips would be necessary

B. Problem Formulation

We consider a wireless network in two-dimensional (2-D) space, and extension to the 3-D case is straightforward. We let, without loss of generality, $\mathcal{S}_a = \{1, 2, \dots, N_l\}$ be the set of indices of the anchors, whose positions $\mathbf{p}_i \in \mathbb{R}^2, \forall i \in \mathcal{S}_a$ are known and fixed, and $\mathcal{S}_b = \{N_l + 1, N_l + 2, \dots, N\}$ be the set of indices of the agents, whose positions are unknown.

In accordance with numerous established studies, e.g., [24], the measured distance between any two nodes i and j can be represented as follows:

$$x_{ij} = d(\mathbf{p}_i, \mathbf{p}_j) + n_{ij}, \quad (1)$$

where $d(\mathbf{p}_i, \mathbf{p}_j) := \|\mathbf{p}_i - \mathbf{p}_j\|$ is defined as the Euclidean distance between nodes (i, j) . n_{ij} accounts for an additive measurement error arising from line-of-sight (LOS) and

non-line-of-sight (NLOS) propagation, and it can be further detailed as follows:

$$n_{ij} = n_{ij}^L + b_{ij}n_{ij}^N. \quad (2)$$

Here, the LOS noise n_{ij}^L follows a zero-mean Gaussian distribution, i.e., $n_{ij}^L \sim \mathcal{N}(0, \sigma^2)$, while the NLOS bias n_{ij}^N is generated from a positive biased distribution, such as the positive uniform distribution. b_{ij} is sampled from the Bernoulli distribution $\mathcal{B}(p_B)$ with p_B being the NLOS occurrence probability. Measured distances can be estimated from the received signal strength (RSS), or time of arrival (ToA) measurements, which can be acquired through diverse technologies, including cellular networks, WLAN, ultra-wideband based on radio frequencies, as well as ultra and audible sound. NLOS propagation introduces significant propagation time delay and substantial signal attenuation for TOA and RSS measurements, respectively [27].

Consequently, a measured distance matrix, denoted by $\mathbf{X} \in \mathbb{R}^{N \times N}$, is constructed by stacking the measured distances, i.e., x_{ij} is the (ij) -th entry of \mathbf{X} . Notably, we consider a symmetric scenario, where $x_{ij} = x_{ji}$, and the measured distance matrix \mathbf{X} adheres to a 'zero-diagonal' property, i.e., $x_{ii} = 0$ for $i = 1, 2, \dots, N$. Based on this measurement matrix, our primary objective is to accurately locate the agents within a massive wireless network with satisfactory computation time. To fulfill this objective, we introduce a completely new learning paradigm, namely GNN-based network localization. This approach is data-driven and leverages a graph-based machine learning model, the details of which will be elaborated upon in the subsequent section.

III. NETWORK LOCALIZATION WITH GCN

In this section, a GCN-based data-driven method is introduced for network localization. Subsequently, we provide key findings regarding the reasons for the exceptional performance of this model. However, we also acknowledge certain limitations that necessitate further improvement.

A. Graph Convolutional Network

Among the various types of GNN models, graph convolutional networks (GCNs) represent a prominent category. In this section, our focus lies in the formulation of the network localization problem utilizing GCNs.

We formally define an undirected graph associated with a wireless network as $\mathcal{G} = (\mathcal{V}, \mathbf{A})$, where \mathcal{V} denotes the vertex set of the nodes $\{v_1, v_2, \dots, v_N\}$, and $\mathbf{A} \in \mathbb{R}^{N \times N}$ is a symmetric adjacency matrix. Each element a_{ij} represents the weight of the edge connecting nodes v_i and v_j . Specifically, we set $a_{ij} = 1$ if there exists a connection between v_i and v_j , otherwise $a_{ij} = 0$. The degree matrix $\mathbf{D} \in \mathbb{R}^{N \times N} := \text{diag}(d_1, d_2, \dots, d_N)$ is a diagonal matrix with $d_i = \sum_{j=1}^N a_{ij}$.

In the original GCN framework, the edge weight a_{ij} can be inherently interpreted as a similarity coefficient between nodes i and j . This concept is particularly relevant in the context of network localization, where the notion of similarity signifies proximity, essentially indicating a small Euclidean distance $d(\mathbf{p}_i, \mathbf{p}_j)$ between nodes. To operationalize this idea, we introduce a Euclidean distance threshold, denoted by T_h , to determine whether an edge exists or not between any two nodes. As further elaborated in Sec. III-B, this threshold plays a crucial role in localization performance. Through thresholding, a refined adjacency matrix $\mathbf{A} \in \mathbb{R}^{N \times N}$ is constructed as follows:

$$a_{ij} = \begin{cases} 0, & \text{if } x_{ij} > T_h \\ 1, & \text{otherwise.} \end{cases} \quad (3)$$

Note that \mathbf{A} already is the augmented adjacency matrix, which includes the self-connection. Furthermore, the associated degree matrix of \mathbf{A} is denoted by $\mathbf{D} \in \mathbb{R}^{N \times N}$. Similarly, we construct a sparse measured distance matrix $\hat{\mathbf{X}} = \mathbf{A} \odot \mathbf{X}$. Consequently, $\hat{\mathbf{X}}$ contains only measured distances that are smaller than or equal to T_h .

In general, each layer of a GCN involves three fundamental actions: feature propagation, linear transformation and element-wise nonlinear activation [28], as illustrated in Fig. 2. The key distinction between GCN and the standard multi-layer perceptron (MLP) [29] lies in the process of feature propagation, which will be clarified in the following.

In the k -th graph convolution layer, let D_k denote the number of neurons in the k -th layer. We represent the input and output node representations as matrices $\mathbf{H}^{(k-1)}$ and $\mathbf{H}^{(k)} \in \mathbb{R}^{N \times D_k}$, respectively. The initial node representations are characterized by $\mathbf{H}^{(0)} = \hat{\mathbf{X}}$. What distinguishes a K -layer GCN from a K -layer MLP is the manner in which the hidden representation of each node in GCN is influenced by its neighbors. More precisely, in GCN, the update process for all layers involves the following matrix multiplication:

$$\bar{\mathbf{H}}^{(k)} \in \mathbb{R}^{N \times D_{k-1}} \leftarrow \hat{\mathbf{A}}\mathbf{H}^{(k-1)}, \quad (4)$$

where $\hat{\mathbf{A}} \in \mathbb{R}^{N \times N} := \mathbf{D}^{-\frac{1}{2}}\mathbf{A}\mathbf{D}^{-\frac{1}{2}}$ signifies the normalized adjacency matrix [1], and $\bar{\mathbf{H}}^{(k)}$ represents the hidden representation matrix in the k -th graph convolution layer. Conceptually, this step effectively smoothens the hidden representations within the local graph neighborhood, thereby promoting similar predictions among closely connected nodes.

Following the feature propagation step, the subsequent two stages of GCN, linear transformation and nonlinear activation, align closely with those employed in standard MLP architectures. Specifically, the k -th layer contains a layer-specific trainable weight matrix $\mathbf{W}^{(k)} \in \mathbb{R}^{D_{k-1} \times D_k}$ and a nonlinear activation function $\sigma(\cdot)$, such as the Rectified Linear Unit $\text{ReLU}(\cdot) = \max(0, \cdot)$ [30]. The update rule for

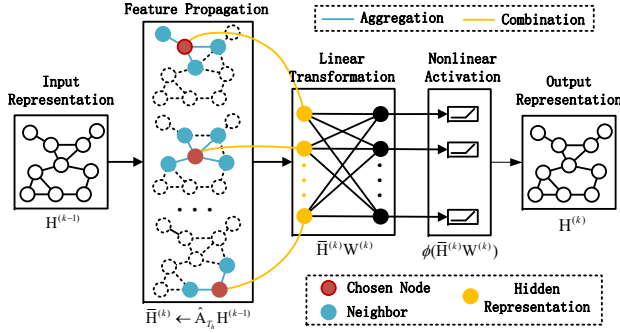


Fig. 2: Diagram of GCN updating rule for single hidden layer.

the representation in the k -th layer is given by:

$$H^{(k)} \leftarrow \sigma \left(\bar{H}^{(k)} W^{(k)} \right). \quad (5)$$

It is noteworthy that the activation function $\sigma(\cdot)$ is applied to every element in the matrix.

Taking a 2-layer GCN as an example, the estimated positions, denoted as $\hat{\mathbf{P}} = [\hat{\mathbf{p}}_1, \hat{\mathbf{p}}_2, \dots, \hat{\mathbf{p}}_N]^\top \in \mathbb{R}^{N \times 2}$, are determined by the following equation:

$$\hat{\mathbf{P}} = \hat{\mathbf{A}} \sigma \left(\hat{\mathbf{A}} \hat{\mathbf{X}} W^{(1)} \right) W^{(2)}. \quad (6)$$

The weight matrices $W^{(1)}$ and $W^{(2)}$ can be optimized by minimizing the mean-squared-error (MSE), defined as $\mathcal{L}(W^{(1)}, W^{(2)}) := \|\mathbf{P}_l - \hat{\mathbf{P}}_l\|_F^2$. Here, $\mathbf{P}_l = [\mathbf{p}_1, \mathbf{p}_2, \dots, \mathbf{p}_{N_l}]^\top$ and $\hat{\mathbf{P}}_l = [\hat{\mathbf{p}}_1, \hat{\mathbf{p}}_2, \dots, \hat{\mathbf{p}}_{N_l}]^\top$ represent the true anchor positions and their estimates, respectively. Then, the optimization problems for GCN-based network localization method can be expressed as follows:

$$\begin{aligned} \arg \min_{\mathbf{W}} \quad & \mathcal{L} = \|\mathbf{P}_l - \hat{\mathbf{P}}_l\|_F^2 \\ \text{s.t.} \quad & \hat{\mathbf{P}} = \text{GCN}_{\mathbf{W}}(\mathbf{A}, \hat{\mathbf{X}}) \\ & [A_{T_h}]_{ij} = \begin{cases} 0, & \text{if } x_{ij} > T_h \\ 1, & \text{otherwise.} \end{cases} \\ & \hat{x}_{ij} = \begin{cases} 0, & \text{if } x_{ij} > T_h \\ x_{ij}, & \text{otherwise.} \end{cases} \end{aligned} \quad (7)$$

Here, \mathbf{W} denotes all trainable matrices in GCN model. To solve this optimization problem, commonly used methods include gradient descent techniques, such as stochastic gradient descent [31] or Adam [32].

B. Key Findings of GCN

The numerical results, as detailed in Section VI, illustrate the substantial advancements realized through the utilization of the GCN-based approach in contrast to several benchmark methods. In the subsequent discussion, we delve into key

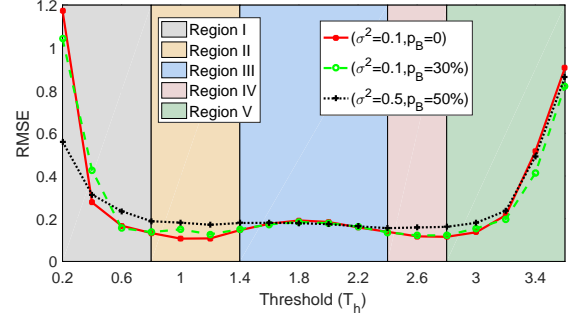


Fig. 3: The averaged loss (RMSE) versus threshold under different noise conditions in GCN model.

findings that shed light on the factors contributing to the remarkable success of this model. These findings offer valuable insights into the efficacy of the GCN-based approach, emphasizing its suitability for network localization.

We pinpoint two major factors: the threshold T_h and the normalized adjacency matrix $\hat{\mathbf{A}}$. In the following, we dissect and explore these factors individually, even though it is worth noting that T_h plays a determinative role in constructing $\hat{\mathbf{A}}$.

1) *Effects of Thresholding*: Thresholding serves two primary functions: 1) the truncation of significant noise, and 2) the prevention of over-smoothing.

Noise truncation. The operation, $\hat{\mathbf{X}} = \mathbf{A} \odot \mathbf{X}$, in Sec. III-A implies that for each $\hat{x}_{ij} \neq 0$, $d(\mathbf{p}_i, \mathbf{p}_j) + n_{ij} \leq T_h$ holds. In simpler terms, for each non-zero element in $\hat{\mathbf{X}}$, we can infer that $n_{ij} \leq T_h - d(\mathbf{p}_i, \mathbf{p}_j)$, signifying that only noise within a confined and limited range is considered within $\hat{\mathbf{X}}$. Specifically, large values of n_{ij} typically result from positive non-line-of-sight (NLOS) bias n_{ij}^N . As a result, each element x_{ij} , associated with either a substantial true distance or a considerable level of noise, is disregarded when the threshold T_h is set to a small value. In essence, this implies that measurements are retained if two nodes are adjacent and primarily affected by a small or moderate measurement noise.

Avoiding over-smoothing. When the threshold is sufficiently large, the corresponding graph becomes fully connected, and the adjacency matrix transforms into a matrix filled with ones. In this scenario, as indicated by Equation (4), all entries within the hidden representation matrix $\bar{H}^{(k)}$ become identical. This signifies that the obtained hidden representation entirely loses its distance-related information. Consequently, the predicted positions of all nodes tend to converge towards a single point. This phenomenon is commonly referred to as over-smoothing. Therefore, it is imperative to select an appropriate threshold to prevent such detrimental effects.

To provide a more comprehensive elucidation of the influence of the threshold, T_h , on the localization performance, we conducted an experiment that systematically explores the RMSE of GCN across a range of T_h within three distinct noise scenarios, as depicted in Fig. 3. This result allows us to categorize the localization performance into five distinct regions, each corresponding to different threshold values. In Region I ($T_h \in [0.2, 0.8]$), the RMSE initially exhibits a large value, followed by a rapid decline as T_h increases. This initial decline in performance can be attributed to the inadequacy of edges in the graph when T_h is set too low, resulting in the presence of isolated nodes.

Within Regions II \sim IV ($T_h \in (0.8, 2.8]$), GCN demonstrates a relatively small fluctuation. A closer inspection reveals that the RMSE is relatively lower in Region II, experiences a slight elevation in Region III, and subsequently decreases in Region IV to reach the same low level as observed in Region II. This nuanced observation can be elucidated as follows. In the range of $T_h \in (0.8, 1.4]$, the commendable performance of GCN can be attributed to the NLOS noise truncation effect of T_h . For $T_h \in (2.4, 2.8]$, the adverse impact of substantial NLOS noise is compensated by the increased number of neighbors for each node. Finally, the abrupt surge in RMSE observed in Region V can be ascribed to the influence of exceptionally high NLOS noise and the phenomenon of over-smoothing.

2) *Effects of $\hat{\mathbf{A}}$* : To comprehend the superior localization performance of GCN, we conduct an analysis of the effects of the normalized adjacency matrix, $\hat{\mathbf{A}}$, from both spatial and spectral perspectives.

Aggregation and combination. To understand the spatial effect of $\hat{\mathbf{A}}$, we disassemble $\hat{\mathbf{A}}$, cf. Eq. (4), into two components:

$$\bar{\mathbf{h}}_{[i,:]}^{(k)} = \underbrace{\frac{1}{d_i} \mathbf{h}_{[i,:]}^{(k-1)}}_{\text{Own information}} + \underbrace{\sum_{j \in \mathcal{N}_i} \frac{a_{ij}}{\sqrt{d_i d_j}} \mathbf{h}_{[j,:]}^{(k-1)}}_{\text{Aggregated information}}. \quad (8)$$

In essence, Eq.(8) encapsulates two critical operations: aggregation and combination. Aggregation, which corresponds to the second term of Eq.(8), captures the features of neighboring nodes by following the given graph structure. Subsequently, the individual node's intrinsic information is combined with the aggregated part.

In contrast to the training process of MLP, which exclusively leverages the characteristics of labeled nodes (referred to anchors in this context), GCN adopts a semi-supervised approach. In GCN, the hidden representation of each labeled node is a weighted summation of those of its neighbors. Equivalently speaking, GCN trains a model by harnessing the attributes of both labeled and unlabeled nodes, thereby contributing to its superior performance in

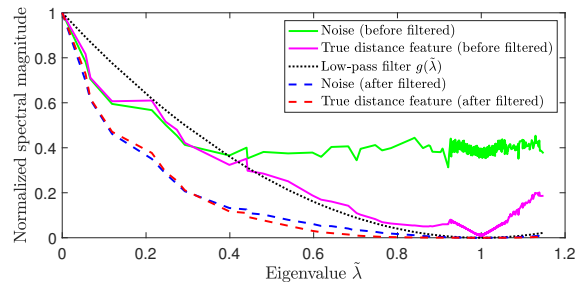


Fig. 4: Spectral components of different signals in dataset ($\sigma^2 = 0.1, p_B = 0$).

network localization.

Low-pass filtering. From the spectral perspective, the eigenvalues of the normalized Laplacian $\tilde{\mathbf{L}} = \mathbf{I} - \hat{\mathbf{A}}$, denoted as $\tilde{\lambda}$, can be interpreted as the "frequency" components [33], [34]. The multiplication of K normalized adjacency matrices $\hat{\mathbf{A}}^K$ across the graph convolution layers is analogous to the application of a spectral "low-pass" filter $g(\tilde{\lambda}_i) := (1 - \tilde{\lambda}_i)^K$, where $\tilde{\lambda}_i, i = 1, 2, \dots$ [28].

Fig. 4 illustrates the "frequency" components of the LOS noise and the true distance matrix before and after filtering. Notably, the majority of information within the true distance matrix (before filtering) is concentrated in the "low-frequency" band, while both "low-frequency" and "high-frequency" components are observable in the LOS noise (before filtering). Consequently, $\hat{\mathbf{A}}$, functioning as a "low-pass" filter, effectively mitigates the "high-frequency" component of the LOS noise. This provides a rationale for the enhanced localization performance of GCNs from a spectral standpoint.

C. Limitations of GCN

From the preceding discussion, it is evident that the proposed GCN-based model exhibits a high degree of suitability for network localization tasks. Nevertheless, the subsequent discussion has uncovered several limitations inherent to this model. Recognizing and subsequently addressing these limitations will be crucial for further enhancing the model's robustness and applicability in real-world scenarios. The primary limitations can be summarized as follows:

Optimal threshold issue. As shown in Fig. 3, the selection of threshold T_h plays a pivotal role in determining the localization performance. However, as a hyperparameter, determining the optimal value for this threshold is not straightforward, particularly in diverse noise and network size scenarios. Consequently, there arises a necessity to develop a flexible model capable of autonomously learning the optimal threshold during the training process. Furthermore, due to the distinct node positions and varying channel state information, each node may possess its unique optimal

threshold, rather than a uniform threshold applicable to all nodes.

Limited model expressiveness. In accordance with Eq. (8), the GCN-based model employs a constant aggregation weight, determined by adjacency and node degree, which constrains its capacity to adaptively aggregate and combine the information from neighboring nodes across the graph structure. From the spectral perspective, the GCN-based model exclusively represents a fixed graph convolutional filter, as delineated by a black dotted line in Fig. 4. This inherent limitation undermines its expressiveness when dealing with intricate network scenarios that necessitate tailored filters at each graph convolutional layer.

Then, we turn our attention to offering effective solutions to mitigate the aforementioned issues by introducing two AGNN models in the subsequent section.

IV. NETWORK LOCALIZATION WITH AGNNS

In this section, we concentrate on the design of two AGNN models that possess the capability to autonomously determine the optimal threshold and adaptively acquire the aggregation weight of each node for various network localization tasks.

A. Attention Mechanism for Network Localization

In the GCN-based localization model, the adjacency matrix \mathbf{A} is constructed based on an Euclidean distance threshold T_h that determines edge connections between two nodes. Each element of the adjacency matrix then acts as a fixed aggregation weight. These factors, namely the sensitivity to the chosen T_h and limited model expressiveness, highlight the limitations of the GCN-based method.

Motivated by recent advancements in attention-based graph neural networks, such as GAT [3] and GATv2 [35], we incorporate the attention mechanism into network localization task. This adaptation is expected to enable the model to automatically determine neighbor sets for each node and acquire flexible aggregation weights for all pairs of nodes based on attention scores.

Every graph attention architecture is typically composed of a series of graph attention layers [3]. In this context, we begin by explaining the fundamental structure of a single graph attention layer. Within each layer, at least one learnable linear transformation is essential to enhance the expressive power, facilitating the transformation of input representations into higher-level ones. This transformation is parameterized by a weight matrix denoted as $\mathbf{W}^{(k-1)} \in \mathbb{R}^{D_{k-1} \times D_k}$ and is applied to every node in the graph. Subsequently, the self-attention on the nodes can be conducted by a shared attentional mechanism, denoted as

$\text{Att}(\cdot, \cdot) : \mathbb{R}^{D_k} \times \mathbb{R}^{D_k} \rightarrow \mathbb{R}$. This mechanism computes attention coefficients, as defined by:

$$e_{ij}^{(k-1)} = \text{Att}(\mathbf{h}_{[i,:]}^{(k-1)} \mathbf{W}^{(k-1)}, \mathbf{h}_{[j,:]}^{(k-1)} \mathbf{W}^{(k-1)}), \quad (9)$$

indicating the importance of node j 's representation concerning node i .

In general, Eq. 9 permits each node to compute an attention score with respect to every other node, treating as a complete graph. However, directly calculating attention scores for all possible node pairs presents two significant challenges:

High computational complexity. As the number of nodes in a complete graph increases, the number of potential edges grows exponentially. Computing attention scores for all possible edges can rapidly become computationally intensive and time-consuming. This issue can significantly slow down the training of the attention mechanism, especially when dealing with large complete graphs.

Over-smoothing issues. In a complete graph, each node's representation necessitates aggregation with those of all other nodes. This comprehensive aggregation results in a convergence of distance-related information across all nodes, ultimately giving rise to the over-smoothing issue. Interestingly, even when assigning varying attention scores to different edges, the graph attention mechanism does not offer an effective safeguard against over-smoothing, and its expressive power diminishes exponentially [36].

This suggests that utilizing the graph attention model directly without taking into account any underlying graph structure—usually assumed to be predefined in existing graph attention models—is not suitable for network localization, where the adjacency of each nodes are typically unknown.

To tackle this challenge, we introduce two novel AGNN models for network localization tasks in the subsequent sections. These models are explicitly crafted to autonomously acquire graph structures during the training process, making them highly suitable for network localization tasks across diverse network scenarios.

B. Overview of AGNN Models

Within this context, we propose two distinct AGNN models tailored for network localization tasks. These models share a common structure comprising Adjacency Learning Modules (ALMs) and multiple graph attention layers, as illustrated in Fig. 5. The ALMs are responsible for automatically learning the adjacent neighbor set for each node by various strategies. Subsequently, the graph attention layers utilize an attention-based mechanism to acquire adaptable aggregation weights based on the learned adjacency matrix.

The distinction between the two AGNNs primarily lies in the specific methodologies employed within the ALMs. Two

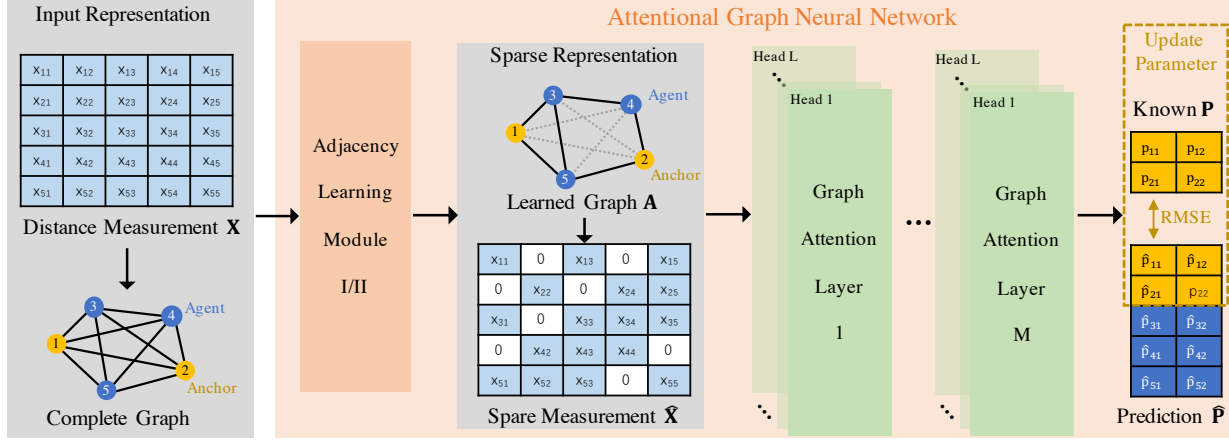


Fig. 5: Framework of AGNN.

ALMs, denoted as ALM-I and NLM-II, are developed based on different foundational principles. ALM-I determines a unique optimal threshold for each individual node during training, as opposed to using a predetermined uniform threshold as in the GCN-based method. ALM-II leverages an attention mechanism to learn a distance-aware threshold. In other words, nodes can adaptively adjust the threshold based on the true distance to their neighbors, enabling more flexible neighbor selection. Both of these methods are capable of learning an adjacency matrix, thereby significantly reducing computational complexity and effectively addressing the over-smoothing issue encountered in graph attention models. Next, we delve into the details of these two types of ALMs.

C. ALM-I (Threshold Learning Method)

In network localization, the adjacency relationships between nodes are typically unknown. Originally, the GCN-based model relies on a manually set threshold T_h , which is uniformly applied to all nodes, to determine adjacency. However, in scenarios characterized by varying noise levels and network sizes, the determination of an appropriate T_h is intractable.

To address this issue related to predetermined thresholds, we introduce a threshold learning method capable of autonomously learning an individual threshold for each node. More precisely, the threshold learning method transforms the threshold into a trainable parameter vector, with each element representing the threshold value for a specific node. This parameter vector can be updated and optimized through backpropagation process. The specific approach is outlined as follows.

The trainable threshold vector is represented as $\mathbf{t}^v \in \mathbb{R}^N$. Since \mathbf{t}^v serves as a trainable parameter vector, it is imperative to ensure that each element within this vector remains within the interval $[0, l_{\max}]$, where l_{\max} corresponds

to the maximum distance at which a node in the network can receive signals. To enforce this constraint on \mathbf{t}^v during the training process, we apply the following rescaling operation:

$$\hat{\mathbf{t}}^v = l_{\max} \cdot \text{sigmoid}(\mathbf{t}^v). \quad (10)$$

Subsequently, similar to Eq. (3), the adjacency matrix $\mathbf{A} \in \mathbb{R}^{N \times N}$ is constructed as follows:

$$a_{ij} = \begin{cases} 0, & \text{if } x_{ij} > \hat{t}_i^v \\ 1, & \text{otherwise.} \end{cases} \quad (11)$$

Additionally, the thresholded measured distance matrix is defined as $\hat{\mathbf{X}} = \mathbf{A} \odot \mathbf{X}$. For each element of $\hat{\mathbf{X}}$, the relationship is expressed as:

$$\hat{x}_{ij} = \begin{cases} 0, & \text{if } x_{ij} > \hat{t}_i^v \\ x_{ij}, & \text{otherwise.} \end{cases} \quad (12)$$

From Eq. (11) and Eq. (12), it is evident that both $\hat{\mathbf{X}}$ and \mathbf{A} are determined by a step function with respect to the threshold. However, because the threshold \hat{t}^v only appears within the conditional statement, and the step function itself lacks differentiability, directly utilizing these equations to compute $\hat{\mathbf{X}}$ and \mathbf{A} would render it impossible to update the parameter vector \mathbf{t}^v through gradient-based optimization. Therefore, it becomes imperative to find a differentiable approximation to the step function.

Conventional methods usually employ a sigmoid function to approximate the step function. However, this approach is not applicable to our problem, given that the threshold is utilized to eliminate elements greater than the threshold to achieve sparse adjacency and distance matrices. The sigmoid function output merely reduces the value of the elements that need to be eliminated, but does not entirely remove them. For instance, the result of $\text{sigmoid}(10) = 4.54 \times 10^{-5}$ is close but not equal to 0. Consequently,

we develop an appropriate approximating step function that addresses this issue. The approximating step function can be defined as follows:

$$\hat{\delta}(x) = \text{ReLU}(\tanh(\gamma x)), \quad (13)$$

where γ represents a constant that adjusts the slope of the hyperbolic tangent (\tanh) function.

Subsequently, the approximation of Eq. (11) and Eq. (12) can be expressed as:

$$a_{ij} = \text{ReLU}(-\tanh(\gamma(x_{ij} - \hat{t}_i^v))) \quad (14)$$

$$\hat{x}_{ij} = x_{ij} \cdot \text{ReLU}(-\tanh(\gamma(x_{ij} - \hat{t}_i^v))). \quad (15)$$

It is evident that our devised approximating step function, employing ReLU and \tanh , yields a notably sharper transition compared to the sigmoid function, consequently achieving a more accurate approximation of the step function. Moreover, its derivative can be obtained everywhere¹. The negative \tanh function within the approximating step function assigns negative values to elements greater than the threshold, while the subsequent ReLU activation function truncates them to zero.

The hyperparameter γ governs the slope of the \tanh function and necessitates appropriate tuning. When γ is too small, some neighboring nodes reside in an intermediate state of the approximating step function, resulting in a slight compression and distortion of their features, resulting in $\hat{x}_{ij} < x_{ij}$. Conversely, a too-large γ can lead to gradient vanishing issues during backpropagation. Our empirical investigations suggest that γ falls within the range of 10 to 1000 for effective threshold vector learning.

Once the learnable adjacency matrix and thresholded measured distance matrix are obtained via the threshold learning method, they can be effectively employed as inputs for the subsequent graph attention layer.

D. ALM-II (Attentional Method)

In ALM-I, the threshold is treated as a trainable vector, allowing each node to set a individual standard for selecting neighbors. However, this method has a potential drawback: assigning a uniform threshold to all neighbors of a node implies neighbors closer to the node may contain larger amounts of noise, as evident from Eq. (1). To overcome this limitation, ALM-II utilizes an attention mechanism to learn a threshold matrix associated with the distances to neighbors. Consequently, it excludes neighbors that are contaminated by NLOS but close in distance, achieving adaptive threshold adjustment. The ALM-II structure consists two components: coarse-grained neighbor selection through a manually set threshold and fine-grained neighbor refinement using the

¹In the standard definition of ReLU, the derivative at 0 is typically considered 0.

attention mechanism. Subsequently, we provide the details of these two components.

To address the challenge of computing attention scores without prior knowledge of the graph structure, we initially utilize a manually set threshold, T_h^0 , to perform coarse-grained neighbor selection for each node, following the procedure in Eq. (3). Notably, unlike the threshold in the GCN-based model, which significantly impacts localization accuracy, the threshold in our primary selection module can be chosen from a broader range. This is because our objective is to establish a coarse-grained neighbor set for each node, thereby reducing computational complexity and alleviating the over-smoothing issue.

To facilitate fine-grained neighbor set learning within each previously identified coarse-grained neighbor set, we introduce a distance-aware threshold matrix based on attention coefficients, enabling further refinement of the previously coarse-grained neighbor set by comparing it to the measured distance values.

Specifically, we incorporate the attention mechanism into the coarse-grained graph structure by employing masked attention—we only compute the coefficient e_{ij}^A only for nodes j within the coarse-grained neighbor set \mathcal{N}_i^C of node i in the graph. Our carefully designed attention coefficient from node j to node i is calculated as follows:

$$e_{ij}^A = |\phi(\mathbf{x}_{[i,:]} \mathbf{W}_A) - \phi(\mathbf{x}_{[j,:]} \mathbf{W}_A)| \mathbf{v}_A, \quad j \in \mathcal{N}_i^C. \quad (16)$$

Here, $|\mathbf{x}|$ represents taking the absolute value of each element in vector \mathbf{x} . The attention mechanism in this context consists of a two-layer neural network, parametrized by an attention weight vector $\mathbf{v}_A \in \mathbb{R}^{F_A}$ and an attention weight matrix $\mathbf{W}_A \in \mathbb{R}^{N \times F_A}$. It applies a nonlinearity function $\phi(\cdot)$, such as LeakyReLU.

The reason for using Eq. 16 to compute attention coefficients, as opposed to a single-layer neural network used in GAT [3] and GATv2 [35], can be explained as follows:

- Passing each node's feature through a linear transformation with \mathbf{W}_A followed by a nonlinear activation function enhances the expressive power of feature transformations;
- The operation of subtracting two transformed representation vectors and then element-wise taking the absolute value intuitively reflects a distance metric between their representations;
- Considering the symmetry property of distances, i.e., $d(\mathbf{p}_i, \mathbf{p}_j) = d(\mathbf{p}_j, \mathbf{p}_i)$, the learned attention coefficients also need to possess permutation invariance, meaning $e_{ij} = e_{ji}$. This property, essential for network localization, is not considered by GAT and GATv2 but can be ensured by our proposed attention mechanism.

To convert the attention coefficient into thresholds and ensure coefficients are easily comparable to measured

distances of different nodes, we apply nonlinear scaling through:

$$T_{ij}^A = \max_{\text{row}}(\mathbf{x}_{[i,:]} \cdot \text{sigmoid}(e_{ij}^A)), \quad (17)$$

where $\max_{\text{row}}(\mathbf{x}_{[i,:]})$ identifies the maximum value from the row vector $\mathbf{x}_{[i,:]}$. Using Eq. (17), we obtain a distance-aware threshold matrix denoted as \mathbf{T}^A . With the distance-aware thresholds obtained within each coarse-grained neighbor set, we establish a criterion for selecting fine-grained neighbors by comparing the measured distance with the thresholds. Specifically, the adjacency and the thresholded measured distance can be represented as follows:

$$a_{ij} \text{ or } \hat{x}_{ij} = \begin{cases} 1 \text{ or } x_{ij}, & \text{if } x_{ij} < T_{ij}^A \\ 0, & \text{otherwise.} \end{cases} \quad (18)$$

Similarly, we adopt the approximating step function used in ALM-I to Eq. (18):

$$a_{ij} = \text{ReLU}(-\tanh(\gamma(x_{ij} - T_{ij}^A))) \quad (19)$$

$$\hat{x}_{ij} = x_{ij} \cdot \text{ReLU}(-\tanh(\gamma(x_{ij} - T_{ij}^A))). \quad (20)$$

After obtaining the adjacency matrix \mathbf{A} and thresholded measured distance matrix $\hat{\mathbf{X}}$ via the attentional method, they can be used as input for the graph attention layer.

E. Graph Attention Layer

We assume that the final neighbor set of each node has been generated through ALM-I/II, denoted as \mathcal{N}_i^F for the fine-grained neighbor set of node i . We subsequently employ the attention mechanism to learn the aggregation weight and predict the positions of all nodes.

We start by describing the k -th single graph attention layer, as the sole layer utilized throughout all of the graph attention architectures used in our model. Here, the attention mechanism $\text{Att}(\cdot, \cdot)$ in Eq. (9) is a single layer feed-forward neural network, parametrized by an attention weight vector $\mathbf{v}_{att}^{(k-1)} \in \mathbb{R}^{F_{att}}$ and an attention weight matrix $\mathbf{W}_{att}^{(k-1)} \in \mathbb{R}^{2D_k \times F_{att}}$, and applying the nonlinearity $\phi(\cdot)$. The coefficients computed by the attention mechanism may then be expressed as:

$$e_{ij}^{(k-1)} = \phi \left(\left[\hat{\mathbf{h}}_{[i,:]}^{(k-1)} \parallel \hat{\mathbf{h}}_{[j,:]}^{(k-1)} \right] \mathbf{W}_{att}^{(k-1)} \right) \mathbf{v}_{att}^{(k-1)}, \quad j \in \mathcal{N}_i^F. \quad (21)$$

where

$$\hat{\mathbf{h}}_{[i,:]}^{(k-1)} = \mathbf{h}_i^{(k-1)} \mathbf{W}^{(k-1)}. \quad (22)$$

Here, $\mathbf{W}^{(k-1)} \in \mathbb{R}^{D_{k-1} \times D_k}$ denotes the weight matrix in the $(k-1)$ -th graph attention layer.

To make coefficients easily comparable across different nodes, we normalize them across all choices of j using the softmax function:

$$\alpha_{ij}^{(k-1)} = \text{softmax}_j(e_{ij}^{(k-1)}) = \frac{\exp(e_{ij}^{(k-1)})}{\sum_{j' \in \mathcal{N}_i^F} \exp(e_{ij'}^{(k-1)})}. \quad (23)$$

Once obtained, the normalized attention coefficients are used to compute a linear combination of the features corresponding to them, to serve as the final output features for every node (after potentially applying a element-wise nonlinearity $\sigma(\cdot)$):

$$\mathbf{h}_{[i,:]}^{(k)} = \sigma \left(\sum_{j \in \mathcal{N}_i^F} \alpha_{ij}^{(k-1)} \hat{\mathbf{h}}_{[j,:]}^{(k-1)} \right). \quad (24)$$

Notably, we use two distinct learnable weight matrices with distinct functions in our approach. On one hand, the weight matrix $\mathbf{W}^{(k-1)}$ is used in both Eq. (21) and Eq. (24). It serves as an initial linear transformation in each layer, converting the input representations into higher-level representations. On the other hand, the weight matrix $\mathbf{W}_{att}^{(k-1)}$ works in conjunction with the weight vector $\mathbf{v}_{att}^{(k-1)}$ and the nonlinearity to construct a single-layer feed-forward network that learns an attentive rule for determining the dependence between each pair of nodes. Such a division of the two weight matrices in our model enhances its flexibility and expressiveness.

To stabilize the learning process of self-attention, we have found extending our mechanism to employ multi-head attention to be beneficial [9]. Specifically, L independent attention mechanisms execute the transformation of Eq. (24), and then their features are concatenated, resulting in the following output feature representation:

$$\mathbf{h}_{[i,:]}^{(k)} = \parallel_{l=1}^L \sigma \left(\sum_{j \in \mathcal{N}_i^F} \alpha_{ij}^{(k-1),l} \hat{\mathbf{h}}_{[j,:]}^{(k-1),l} \right) \quad (25)$$

where $\alpha_{ij}^{(k-1),l}$ are normalized attention coefficients computed by the l -th attention mechanism in the $(k-1)$ -th layer, and $\hat{\mathbf{h}}_{[j,:]}^{(k-1),l}$ is the corresponding transformed representation of node j . Note that, in this setting, the final returned output, $\mathbf{h}_{[i,:]}^{(k)}$, will consist of $L * D_K$ features (rather than D_K) for each node.

Specially, if we perform multi-head attention on the final (prediction) layer of the network, concatenation is no longer sensible—instead, we employ averaging, and applying the final nonlinearity until then:

$$\hat{\mathbf{p}}_i^\top = \mathbf{h}_{[i,:]}^{(K)} = \sigma \left(\frac{1}{L} \sum_{l=1}^L \sum_{j \in \mathcal{N}_i^F} \alpha_{ij}^{(K-1),l} \hat{\mathbf{h}}_j^{(K-1),l} \right). \quad (26)$$

F. Optimization Problems for AGNNs

In summary, we propose two ALMs (threshold learning method and attentional method respectively) that can automatically learn an adjacency matrix and a threshold measured distance matrix. Then, we employ the learned two matrices in the graph attention layer.

Here, we present the optimization problems for AGNN-I and AGNN-II. For simplicity, we denote multi graph attention layers, as illustrated in Sec. IV-E, as MGAL. Additionally, the combination of ALM-I/II and MGAL can be denoted as AGNN-I/II.

The optimization problem for AGNN-I can be formulated as follows:

$$\begin{aligned} \arg \min_{\mathbf{W}, \mathbf{t}^v} \quad & \mathcal{L} = \|\mathbf{P}_l - \hat{\mathbf{P}}_l\|_F^2 \\ \text{s.t.} \quad & \hat{\mathbf{P}} = \text{MGAL}_{\mathbf{W}}(\mathbf{A}, \hat{\mathbf{X}}) \\ & a_{ij} = \text{ReLU}(-\tanh(\gamma(x_{ij} - \hat{t}_i^v))) \\ & \hat{x}_{ij} = x_{ij} \cdot \text{ReLU}(-\tanh(\gamma(x_{ij} - \hat{t}_i^v))). \\ & \hat{t}^v = l_{\max} \cdot \text{sigmoid}(\mathbf{t}^v). \end{aligned} \quad (27)$$

Here, \mathbf{W} represents all trainable matrices in MGAL.

In addition, the optimization problem for AGNN-II can be expressed as follows:

$$\begin{aligned} \arg \min_{\mathbf{W}_1, \mathbf{W}_2} \quad & \mathcal{L} = \|\mathbf{P}_l - \hat{\mathbf{P}}_l\|_F^2 \\ \text{s.t.} \quad & \hat{\mathbf{P}} = \text{MGAL}_{\mathbf{W}_1}(\mathbf{A}, \hat{\mathbf{X}}) \\ & \mathbf{A}, \hat{\mathbf{X}} = \text{ALM-II}_{\mathbf{W}_2}(\mathbf{X}, T_h^0) \end{aligned} \quad (28)$$

Here, \mathbf{W}_1 and \mathbf{W}_2 denote all trainable matrices in MGAL and ALM-II, respectively.

V. FUNDAMENTAL PROPERTY ANALYSIS

In this section, we analyze our proposed AGNN-I/II models from the perspectives of three fundamental properties: dynamic attention property, graph signal denoising, and complexity analysis. Through theoretical examination, we aim to elucidate the reasons behind the superior performance of AGNN-I/II in terms of model representational capacity, robustness, and computational complexity.

A. Dynamic Attention Property

In this subsection, we firstly adhere to the precise definitions of static and dynamic attention, given in [35]. Subsequently, we demonstrate that, compared with the classical GAT [3] model which can only calculate static attention and thus suffers from a significant limitation, our proposed graph attention mechanisms in ALM-II (Eq. (16)) and MGAL (Eq. (21, 22)) inherit the dynamic attention property.

In general, attention serves as a mechanism to compute a distribution over a set of input key vectors when provided with an additional query vector. In the context of network

localization, the query vector and input key vectors represent the feature vectors of a given node and its neighbors, respectively. The attention mechanism, in this context, involves the process of learning how to allocate attention weights to all neighboring nodes concerning the target node.

Notably, for the sake of clarity, in the subsequent definitions and proofs, we adopt a scenario involving a complete graph. In this scenario, the neighbor set of each node encompasses all nodes, ensuring that the neighbor set of each node is both maximal and identical. In real-world scenarios featuring non-complete graphs, analogous definitions and proofs can be applied. The key distinction lies in the fact that in such scenarios, the neighbor set of a node becomes a subset of the original one.

When the attention function consistently assigns a weight to one neighbor that is at least as significant as any other neighbors, regardless of the feature vector of target node, we refer to this type of attention function as static [35]:

Definition 1 (Static attention): A (possibly infinite) family of functions $\mathcal{F} \subseteq (\mathbb{R}^{D_k} \times \mathbb{R}^{D_k} \rightarrow \mathbb{R})$ computes attention coefficients for a set of feature vectors nodes $\mathcal{Q} = \{\mathbf{q}_1, \dots, \mathbf{q}_N\} \subset \mathbb{R}^{D_k}$ and those of their neighbors $\mathcal{K} = \{\mathbf{k}_1, \dots, \mathbf{k}_N\} \subset \mathbb{R}^{D_k}$. If for every $f \in \mathcal{F}$, there exists a ‘‘highest coefficient’’ neighbor $j_f \in [N]$ such that for every node $i \in [N]$ and neighbor $j \in [N]$ it holds that $f(\mathbf{q}_i, \mathbf{k}_{j_f}) \geq f(\mathbf{q}_i, \mathbf{k}_j)$. We say that a family of attention functions computes static attention, given \mathcal{K} and \mathcal{Q} .

Static attention is very limited because every function $f \in \mathcal{F}$ has a neighbor that is always selected, regardless of the node. Such functions cannot model situations where different neighbors have different relevance to different nodes. The general and powerful form of attention is dynamic attention [35]:

Definition 2 (Dynamic attention): A (possibly infinite) family of functions $\mathcal{F} \subseteq (\mathbb{R}^{D_k} \times \mathbb{R}^{D_k} \rightarrow \mathbb{R})$ computes attention coefficients for a set of feature vectors nodes $\mathcal{Q} = \{\mathbf{q}_1, \dots, \mathbf{q}_N\} \subset \mathbb{R}^{D_k}$ and those of their neighbors $\mathcal{K} = \{\mathbf{k}_1, \dots, \mathbf{k}_N\} \subset \mathbb{R}^{D_k}$. If for any mapping $\varphi : [N] \rightarrow [N]$, there exists $f \in \mathcal{F}$ such that for any node $i \in [N]$ and any neighbor $j_{\neq \varphi(i)} \in [N]$: $f(\mathbf{q}_i, \mathbf{k}_{\varphi(i)}) > f(\mathbf{q}_i, \mathbf{k}_j)$. We say that a family of attention functions computes dynamic attention for \mathcal{K} and \mathcal{Q} .

That is, dynamic attention can select every neighbor $\varphi(i)$ using the node i , by making $f(\mathbf{q}_i, \mathbf{k}_{\varphi(i)})$ the maximal in $\{f(\mathbf{q}_i, \mathbf{k}_j) \mid j \in [N]\}$.

The motivation of GAT is to compute a representation for every node as a weighted average of its neighbors. A scoring function $e(\mathbf{h}_i, \mathbf{h}_j)$ computes a score for every edge (j, i) , which indicates the importance of the features of the neighbor j to the node i :

$$e(\mathbf{h}_{[i,:]}, \mathbf{h}_{[j,:]}) = \phi([\mathbf{W}\mathbf{h}_{[i,:]} \parallel \mathbf{W}\mathbf{h}_{[j,:]}] \mathbf{v}). \quad (29)$$

Nonetheless, the authors of [35] have proved:

Theorem 1: A GAT layer computes only static attention, for any set of node representations $\mathcal{K} = \mathcal{Q} = \{\mathbf{h}_{[1,:]}, \dots, \mathbf{h}_{[N,:]}\}$. In particular, for $N > 1$, a GAT layer does not compute dynamic attention.

Proof: See App. VIII-A or refer to [35]. ■

The consequence of Thm. 1 is that for any set of nodes \mathcal{V} and a trained GAT layer, the attention function $e(\cdot, \cdot)$ defines a constant ranking (argsort) of the neighbors, unconditioned on the node i . This global ranking induces the local ranking of every neighborhood \mathcal{N}_i . The only effect of \mathbf{h}_i is in the “sharpness” of the produced attention distribution.

The authors of [3] find that utilizing H attention heads and aggregating their outputs through concatenation, similar to the Transformer [9], can lead to improved performance. In this context, Thm. 1 applies individually to each head: for every head $h \in [H]$, there exists (possibly different) nodes that maximize $s_j^{(h)} \mid j \in \mathcal{V}$, and the final output is the concatenation of the outputs from the H static attention heads.

The main problem in scoring function of the standard GAT is that the learned weights, \mathbf{W} and \mathbf{v} , are applied consecutively, and thus can be collapsed into a single linear layer. Compared with the standard GAT, the each graph attention layer in MGAL simply applies the learnable weight vector \mathbf{v}_{att} after the nonlinearity $\phi(\cdot)$, and an additional weight matrix \mathbf{W}_{att} after the concatenation. Next, we show that our proposed graph attention layer can fix this limitation of static attention in GAT and it has a strictly more expressive attention mechanism.

Theorem 2: The graph attention function in Eq. (21, 22) computes dynamic attention for any set of node representations $\mathcal{K} = \mathcal{Q} = \{\mathbf{h}_{[1,:]}, \dots, \mathbf{h}_{[N,:]}\}$.

Proof: See App. VIII-B. ■

The core idea presented in this proof around the notion that the graph attention function in Eq. (21, 22) can be interpreted as a single-layer graph neural network. Consequently, it can be approximated to represent an appropriate function, thereby achieving dynamic attention in accordance with the universal approximation theorem [37]. In contrast, the GAT lacks the capability to approximate any such desired function, as conclusively demonstrated in Thm. 1.

In addition, within ALM-II, we have devised a graph attention function, as depicted in Eq. (16), with the specific goal of implementing a distance-aware attention mechanism. Through a comprehensive analysis, we can confidently assert that this function also demonstrates the dynamic attention property, which is a crucial aspect of its effectiveness.

Theorem 3: The graph attention function in Eq. (16) computes dynamic attention for any set of node representations $\mathcal{K} = \mathcal{Q} = \{\mathbf{x}_{[1,:]}, \dots, \mathbf{x}_{[N,:]}\}$.

Proof: See App. VIII-C. ■

Overall, our proposed graph attention mechanisms in ALM-II and MGAL inherit the dynamic attention property, making them inherently more expressive than the standard GAT.

B. GNNs as Graph Signal Denoising

In this subsection, our objective is to establish the connections between MGAL and a graph signal denoising problem incorporating Laplacian regularization. To achieve this, we begin by referring to the definition of a graph signal denoising problem, as outlined in [38].

Definition 3 (Graph Signal Denoising): Given a noisy signal $\mathbf{S} \in \mathbb{R}^{N \times D_k}$ on a graph \mathcal{G} , the goal is to recover a clean signal $\mathbf{S}' \in \mathbb{R}^{N \times D_k}$, assumed to be smooth over \mathcal{G} , by solving the following optimization problem:

$$\arg \min_{\mathbf{S}'} \mathcal{L} = \|\mathbf{S}' - \mathbf{S}\|_F^2 + c \cdot \text{tr}((\mathbf{S}')^\top \mathbf{L} \mathbf{S}'). \quad (30)$$

The first term guides \mathbf{S}' to be close to \mathbf{S} , while the second term $\text{tr}((\mathbf{S}')^\top \mathbf{L} \mathbf{S}')$ is the Laplacian regularization which guides the smoothness of \mathbf{S}' over \mathcal{G} , with $c > 0$. Assuming that we adopt the unnormalized Laplacian matrix with $\mathbf{L} = \mathbf{D} - \mathbf{A}$ (the adjacency matrix \mathbf{A} is assumed to be binary), the second term in Eq. (30) can be written in either an edge-centric way or a node-centric way as:

$$\text{Edge-centric: } c \sum_{(i,j) \in \mathcal{E}} \left\| \mathbf{s}'_{[i,:]} - \mathbf{s}'_{[j,:]} \right\|^2; \quad (31)$$

$$\text{Node-centric: } \frac{c}{2} \sum_{i \in \mathcal{V}} \sum_{j \in \mathcal{N}(i)} \left\| \mathbf{s}'_{[i,:]} - \mathbf{s}'_{[j,:]} \right\|^2. \quad (32)$$

Clearly, from the edge-centric view, the regularization term measures the global smoothness of \mathbf{S}' , which is small when connected nodes share similar features. On the other hand, from the node-centric view, we can view the term $\sum_{j \in \mathcal{N}(i)} \left\| \mathbf{s}'_{[i,:]} - \mathbf{s}'_{[j,:]} \right\|^2$ as a local smoothness measure for node i as it measures the difference between node i and all its neighbors. The regularization term can then be regarded as a summation of local smoothness over all nodes.

Based on Def. 3, the authors of [38] show the connection between aggregation operation in GCN model and the graph signal denoising. The main result is summarized as follows:

Theorem 4: When the normalized Laplacian matrix $\hat{\mathbf{L}} = \mathbf{I} - \hat{\mathbf{A}}$ is adopted, the feature aggregation operation in GCN (Eq. (4)) can be regarded as solving the optimization problem (Eq. (30)) using one-step gradient descent with $\mathbf{H}^{(k-1)}$ as the input noisy signal and stepsize $b = \frac{1}{2c}$.

Proof: See App. VIII-D or refer to [38]. ■

With this connection, we can verify that a GCN model with multiple GCN layers can be regarded as solving the graph signal denoising problem in multiple times with different noisy signals. Specifically, in the k -th layer, the

aggregation operation aims to solve Eq. (30) with $\mathbf{H}^{(k-1)}$ and $\mathbf{H}^{(k)}$ as input noisy graph signal and the recovered graph signal, respectively.

To establish the connection between graph signal denoising and MGAL, we rewrite the denoising problem in Eq. (30) from a node-centric view as:

$$\arg \min_{\mathbf{s}'} \sum_{i \in \mathcal{V}} \|\mathbf{s}'_{[i,:]} - \mathbf{s}_{[i,:]} \|^2 + \frac{c}{2} \sum_{i \in \mathcal{V}} \sum_{j \in \mathcal{N}(i)} \|\mathbf{s}'_{[i,:]} - \mathbf{s}'_{[j,:]} \|^2. \quad (33)$$

Here, the constant c is shared by all nodes, which indicates that the same level of local smoothness is enforced to all nodes. By relaxing this assumption, instead of a unified c as in Eq. (33), we can consider a node-dependent c_i for each node i :

$$\arg \min_{\mathbf{s}'} \sum_{i \in \mathcal{V}} \|\mathbf{s}'_{[i,:]} - \mathbf{s}_{[i,:]} \|^2 + \sum_{i \in \mathcal{V}} \frac{c_i}{2} \sum_{j \in \mathcal{N}(i)} \|\mathbf{s}'_{[i,:]} - \mathbf{s}'_{[j,:]} \|^2. \quad (34)$$

Subsequently, the authors of [38] show that the aggregation operation of MGAL model (Eq. (24)) is closely connected to an approximate solution of Eq. (34) with the help of Thm. 5.

Theorem 5: With adaptive stepsize $b_i = 1 / \sum_{j \in \mathcal{N}(i)} (c_i + c_j)$ for each node i , the process of taking one step of gradient descent from \mathbf{S} to solve Eq. (34) is as follows:

$$\mathbf{s}'_{[i,:]} \leftarrow \sum_{j \in \mathcal{N}(i)} b_i (c_i + c_j) \mathbf{s}_{[j,:]} \quad (35)$$

Proof: See App. VIII-E or refer to [38]. ■

Eq. (35) resembles the aggregation operation of MGAL, as shown in Eq. (24), if we treat $b_i(c_i + c_j)$ as the attention score α_{ij} . Note that $\sum_{j \in \mathcal{N}(i)} (c_i + c_j) = 1/b_i, \forall i \in \mathcal{V}$. Thus, $(c_i + c_j)$ can be regarded as the unnormalized attention score and b_i as the normalization constant.

Moreover, we compare $b_i(c_i + c_j)$ with α_{ij} by investigating the formulation of e_{ij} in Eq. (21), which can be rewritten as:

$$e_{ij} = \phi \left(\hat{\mathbf{h}}_{[i,:]} \mathbf{W}_{att}^l + \hat{\mathbf{h}}_{[j,:]} \mathbf{W}_{att}^r \right) \mathbf{v}_{att}. \quad (36)$$

Here, $\mathbf{W}_{att}^l \in \mathbb{R}^{D_k \times F}$ and $\mathbf{W}_{att}^r \in \mathbb{R}^{D_k \times F}$ respectively denote the left and right submatrices of the attention weight matrix \mathbf{W}_{att} as defined in Eq. (21).

Comparing e_{ij} with $(c_i + c_j)$, we find that they take a similar form. Specifically, the form of $\hat{\mathbf{h}}_{[i,:]} \mathbf{W}_{att}^l$ and $\hat{\mathbf{h}}_{[j,:]} \mathbf{W}_{att}^r$ (then employing nonlinear activation and taking product with \mathbf{v}_{att}) can be regarded as the approximations of c_i and c_j , respectively. In this way, e_{ij} can be considered as a learnable function estimating $c_i + c_j$. Correspondingly, $b_i(c_i + c_j)$ and α_{ij} are the normalized versions of $c_i + c_j$ and e_{ij} , respectively. The difference between $b_i(c_i + c_j)$ and

α_{ij} is that the normalization in Eq. (35) for $b_i(c_i + c_j)$ is achieved via summation rather than a softmax in Eq. (23) for α_{ij} . Note that similarly to multi-layer GCN, the MGAL can be also regarded as solving a series of graph denoising problems in Eq. (34).

Thus, based on [38], we have demonstrated that both GCN and MGAL can act as solving a series of graph denoising problems. Besides, compared with GCN model, MGAL owns more flexible denoising property, which is consistent with the experimental results.

C. Complexity Analysis

From a computational perspective, our proposed AGNN-I and AGNN-II exhibit high efficiency. The operation of the graph attention layer in MGAL can be parallelized across all edges, and the computation of output features can similarly be parallelized across all nodes. Notably, these models obviate the need for computationally expensive matrix operations, such as eigen-decompositions, which are typically mandatory in spectral-based methods [39], [40].

Furthermore, we provide the time complexity analysis for GCN-based localization models as follows:

Theorem 6: For the k -th graph convolutional layer, the time complexity can be summarized as $O(ND_{k-1}D_k + |E|D_{k-1})$, where $|E|$ represents the numbers of graph edges constructed based on a given threshold.

Proof: See App. VIII-F or refer to [1]. ■

Crucially, the time complexity for our proposed AGNN-I/II is presented as follows:

Theorem 7: The time complexities for ALM-I and ALM-II are $O(N)$ and $O(NNF_A + |E^C|F_A)$, respectively. For the k -th graph attention layer of MGAL, the time complexity can be summarized as $O(ND_kF_{att} + ND_{k-1}D_k + |E^F|F_{att} + |E^F|D_k)$, where $|E^C|$ and $|E^F|$ denote the numbers of edges in the coarse-grained and fine-grained neighbor sets, respectively.

Proof: See App. VIII-G. ■

If we make the assumptions that F_{att} , D_{k-1} , D_k , and N are approximately equal and that $|E|$, $|E^C|$, and $|E^F|$ are also roughly equivalent, then the time complexity of our proposed AGNN-I/II is comparable to that of the baseline GCN-based model. It's worth noting that when applying multi-head attention, the storage and parameter requirements increase by a factor of K , but the computations of individual heads are entirely independent and can be effectively parallelized.

VI. NUMERICAL RESULTS

In this section, we assess the performance of several proposed GNN-based methods in terms of their localization accuracy, robustness against NLOS noise, and computational time. To facilitate meaningful comparisons, we consider

TABLE I: The simulated localization scenarios and implementation details.

Scenarios	Size: 5m×5m		Nodes (Anchors): 500 (20-160)		
Model	Layers	Hidden size	Epochs	Learning rate	Dropout
	2	2000	200	0.01	0.5
Threshold	$T_h = 1.2$ for GCN and MLP Random initialized \mathbf{t}^v for ALM-I, $T_h^0 = 4.0$ for ALM-II $T_h = 0.6$ for competitors (similar performance, less complexity)				

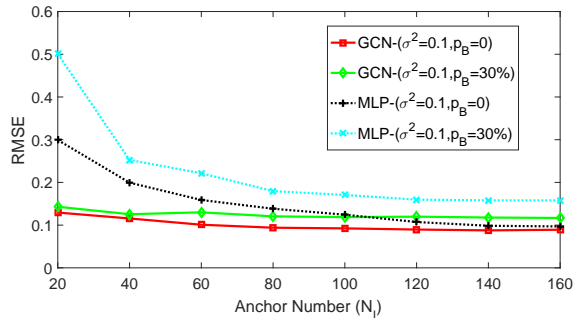


Fig. 6: The averaged loss (RMSE) versus the number of anchors under different noise conditions.

several well-established competitors, including an MLP-based method, the sparsity-inducing semi-definite programming (SDP) method [23], the expectation-conditional maximization (ECM) method [21], and the centralized least-square (LS) method [14]. Note that we incorporate the MLP model into our evaluation to illustrate the performance enhancements attributed to the inclusion of the normalized adjacency matrix, $\hat{\mathbf{A}}$, in each GNN layer.

Simulated localization scenarios and implementation details of our proposed models as well as competitors are shown in Tab. I. The measurement error, n_{ij} , is formulated as $n_{ij} = n_{ij}^L + b_{ij}n_{ij}^N$. Here, the LOS noise, n_{ij}^L , is generated from a zero-mean Gaussian distribution, i.e., $n_{ij}^L \sim \mathcal{N}(0, \sigma^2)$. Concurrently, the positive NLOS bias, n_{ij}^N , is generated from a uniform distribution, $n_{ij}^N \sim \mathcal{U}[0, 10]$. The variable b_{ij} follows a Bernoulli distribution $\mathcal{B}(p_B)$ where p_B represents the probability of NLOS occurrence.

First, we assess the localization accuracy of all methods under different noise conditions. Here, the localization accuracy is measured in terms of the averaged test root-mean-squared-error (RMSE), $\mathcal{L}_R := \|\mathbf{R}_u - \hat{\mathbf{R}}_u\|_F$, where $\mathbf{R}_u = [\mathbf{p}_{N_l+1}, \mathbf{p}_{N_l+2}, \dots, \mathbf{p}_N]^T$ and $\hat{\mathbf{R}}_u = [\hat{\mathbf{p}}_{N_l+1}, \hat{\mathbf{p}}_{N_l+2}, \dots, \hat{\mathbf{p}}_N]^T$. The results are summarized in Table II. It is shown that among all considered methods, GCN provides the highest localization accuracy in almost all cases. In particular, when the NLOS probability, p_B , is high, GCN outperforms all competitors by far. Moreover, we test the localization performance of GCN for large networks with $N = 1000$, denoted by GCN₁₀₀₀ in Table II. The

results show that GCN performs even better with slightly increased computational time, as shown in Table III. If we increase N even further, GCN-based method can maintain its outstanding performance, but other methods (SDP, ECM and LS) will degrade severely in terms of both localization accuracy and computational time.

Next, we focus on two data-driven methods, GCN and MLP, which perform relatively well in Table II. The localization accuracy is investigated by varying N_l from 20 to 160 with a stepsize of 20 under two different noise conditions. The results are depicted in Fig. 6. There are two main observations. First, GCN attains the lowest RMSE consistently for all N_l . Compared with MLP, the improvement in localization accuracy is particularly remarkable for GCN with small N_l . This result indicates that GCN can better exploit the distance information than MLP. When N_l increases, both GCN and MLP tend to approach a performance lower bound. Second, GCN performs similarly under both noise conditions, while MLP shows a clear performance degradation when p_B increases. This observation indicates that GCN is very robust against NLOS. Lastly, we want to mention that a fine-tuned MLP is often superior to NTK which corresponds to random initialized MLP, which performs surprisingly close to other benchmark methods as shown in Table II.

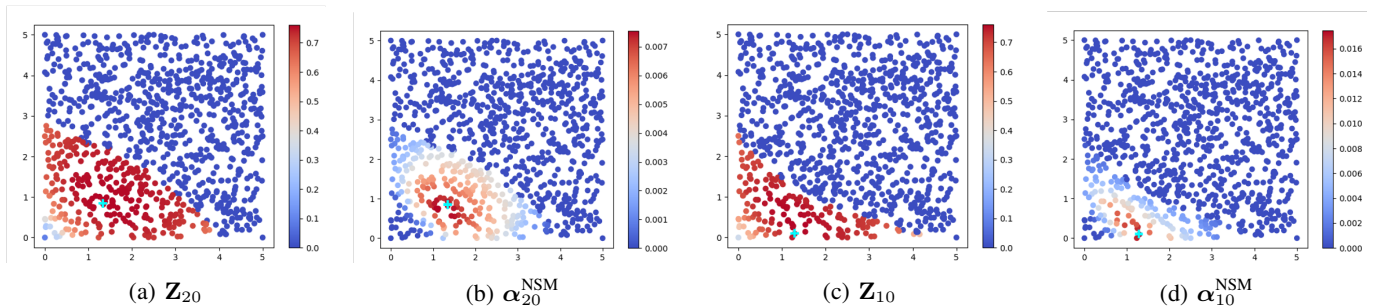
Another important requirement for real-world applications is fast response. Table III shows the practical computational time of different methods. It is shown Besides, the computational time of GCN₁₀₀₀ slightly increases when we double the number of nodes in the network. GCN can also deal with very large network, for instance $N = 10000$, in an affordable time, while the LS, ECM and SDP are all disabled. All above results indicate that the proposed GCN-based method is a prospective solution to large-scale network localization.

The attention architecture has several interesting properties:

- The NSM-II (attentional method) learns a integrated attention matrix α based on the coarse-grained neighbor set. The attention matrix can be regarded as a further refinement of the coarse-grained neighbor set, resulting in a fine-grained adjacency matrix and a threshold measured distance matrix. The Fig. 7 depicts the heat maps of the similarity and integrated attention scores between the 20-th node and all other nodes, and between the 10-th node and all other nodes, respectively. It exemplifies the capacity of the attention mechanism to refine the coarse-grained neighbor sets.
- Besides, the comparison of the attention score distributions between the 20-th and the 10-th nodes, as shown in Fig. 7b and Fig. 7d, reveals that nodes can selectively attend to different numbers and ranges of neighbors, implying that each node can learn an individual optimal threshold. The ability of each node attending to

TABLE II: The averaged loss (RMSE) of all methods under different noise conditions for $N_l=50$.

Methods \ Noise (σ^2, p_B)	(0.04, 0%)	(0.1, 10%)	(0.25, 10%)	(0.25, 30%)	(0.5, 50%)
LS [14]	0.2270	0.2675	0.3884	0.4187	0.7992
ECM [21]	0.1610	0.1857	0.3298	0.3824	0.8011
SDP [23]	0.1171	0.2599	0.4891	0.4641	0.9294
MLP	0.1865	0.1769	0.2305	0.2623	0.3358
GCN	0.1038	0.1128	0.1006	0.1302	0.1755
AGNN-I	0.0677	0.0732	0.0779	0.0817	0.1290
AGL-II	0.0486	0.0551	0.0638	0.0812	0.1015

Fig. 7: Similarity (\mathbf{Z}) vs. attention score (α^{ALM}) in NSM-II for 10-th and 20-th nodes.TABLE III: A comparison of different methods in terms of computational time (in second) at ($\sigma^2 = 0.1, p_B = 30\%$) and $N_l = 50$.

GCN	GCN ₁₀₀₀	GCN ₁₀₀₀₀	MLP	NTK	LS	ECM	SDP
3.24	5.82	707.38	2.05	2.33	32.47	82.85	1587

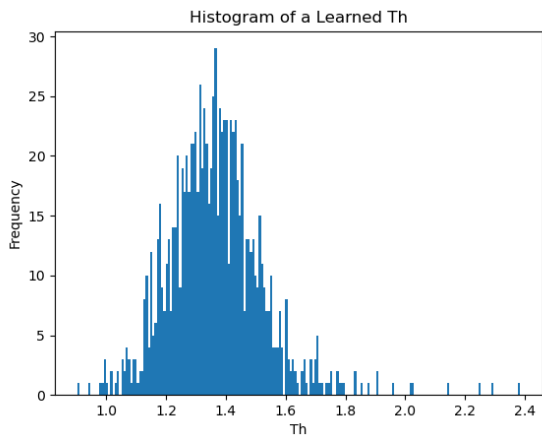


Fig. 8: The histogram of learned thresholds for all nodes in AGL-I.

different neighbors based on its own input features is referred to dynamic attention. In the forthcoming Section V-A, we will present a precise mathematical

definition of dynamic attention and demonstrate that our proposed graph attentional method, employed in both NSM-II and the graph attention layer, possesses this characteristic.

- As shown in Tab., the AGL-0 model outperforms the GCN-based model significantly under all noise conditions. This can be explained in two perspectives. On the one hand, as opposed to GCN-based model, the graph attention layer in AGL model allows for (implicitly) assigning different importance to nodes of a same neighborhood, enabling a leap in model capacity. On the other hand, compared with GCN model, the graph attention layer in AGL model owns more flexible denoising property, which will be illustrated in the following Sec. V-B.
- The AGL-I always outperforms the other models significantly under different noise conditions. This results not only demonstrate the greater potential of graph attention mechanisms but also suggest that each node owns an individual optimal threshold and therefore regarding the threshold of each node as a trainable parameter can achieve less localization errors compared to the AGL-0 model that sets a uniform threshold for all nodes. This can be verified in Fig. 8.
- However, AGL-II only outperforms the GCN-based model under mild noise condition. The reason for this result is that AGL-II uses the attention mechanism to compute the attention score between the feature vectors of two nodes. In the NLOS scenarios, the feature

vectors are subject to significant noise interference, which affects the accuracy of the attention mechanism and leads to attention scores that differ from the true adjacency relationships, thereby reducing the model's performance.

VII. CONCLUSION

In this paper, we mainly focus on the localization problem in large-scale dynamic wireless networks. Firstly, we consider a simple static network localization task. We have proposed a GCN-based data-driven method for robust large-scale network localization in mixed LOS/NLOS environments. Numerical results have shown that the proposed method is able to achieve substantial improvements in terms of localization accuracy, robustness and computational time, in comparison with both MLP and various benchmark methods. For dynamic wireless network localization scenarios, two types of GAL models are proposed to automatically locate all agents without any manual hyperparameter and they can achieve higher localization accuracy than the GCN model. Additionally, we demonstrate that the proposed AGL models have dynamic attention property and more flexible signal denoising property than GCN model. Finally, in order to address the high memory requirement and computation complexity in large-scale networks, we adapt the distributed learning framework for the AGL model.

VIII. APPENDIX

A. Proof of Theorem 1

Let $\mathcal{G} = (\mathcal{V}, \mathcal{E})$ be a graph modeled by a GAT layer with some \mathbf{v} and \mathbf{W} values, and having node representations $\{\mathbf{h}_{[i,:]}, \dots, \mathbf{h}_{[N,:]}\}$. The learned parameter \mathbf{v} can be written as a concatenation $\mathbf{v} = [\mathbf{v}_1 \| \mathbf{v}_2] \in \mathbb{R}^{2D_k}$ such that $\mathbf{v}_1, \mathbf{v}_2 \in \mathbb{R}^{D_k}$, and GAT can be re-written as:

$$e(\mathbf{h}_{[i,:]}, \mathbf{h}_{[j,:]}) = \phi(\mathbf{h}_{[i,:]} \mathbf{W} \mathbf{v}_1 + \mathbf{h}_{[j,:]} \mathbf{W} \mathbf{v}_2). \quad (37)$$

Since \mathcal{V} is finite, there exists a node $j_{max} \in \mathcal{V}$ such that $\mathbf{h}_{[j_{max},:]} \mathbf{W} \mathbf{v}_1$ is maximal among all nodes $j \in \mathcal{V}$ (j_{max} is the j_f required by static). Due to the monotonicity of $\phi(\cdot)$ and softmax, for every query node $i \in \mathcal{V}$, the node j_{max} also leads to the maximal value of its attention distribution $\{\alpha_{ij} \mid j \in \mathcal{V}\}$. Thus, it directly computes only static attention.

B. Proof of Theorem 2

Let $\mathcal{G} = (\mathcal{V}, \mathcal{E})$ be a graph modeled by our proposed graph attention layer, having transformed node representations $\{\mathbf{W} \mathbf{h}_{[i,:]}, \dots, \mathbf{W} \mathbf{h}_{[N,:]}\}$, and let $\varphi : [N] \rightarrow [N]$ be any node mapping $[N] \rightarrow [N]$. We define $g : \mathbb{R}^{2D_k} \rightarrow \mathbb{R}$ as follows:

$$g(\mathbf{x}) = \begin{cases} 1 & \exists i : \mathbf{x} = [\mathbf{W} \mathbf{h}_{[i,:]} \| \mathbf{W} \mathbf{h}_{[\varphi(i),:]}] \\ 0 & \text{otherwise} \end{cases} \quad (38)$$

Next, we define a *continues* function $\tilde{g} : \mathbb{R}^{2D_k} \rightarrow \mathbb{R}$ that equals to g in only specific N^2 inputs:

$$\tilde{g}([\mathbf{h}_{[i,:]} \mathbf{W} \| \mathbf{h}_{[j,:]} \mathbf{W}]) = g([\mathbf{h}_{[i,:]} \mathbf{W} \| \mathbf{h}_{[j,:]} \mathbf{W}]), \forall i, j \in [n]. \quad (39)$$

For all other inputs $x \in \mathbb{R}^{2D_k}$, $\tilde{g}(x)$ realizes to any values that maintain the continuity of \tilde{g} (this is possible because we fixed the values of \tilde{g} for only a finite set of points).²

Thus, for every node $i \in \mathcal{V}$ and $j \neq \varphi(i) \in \mathcal{V}$:

$$1 = \tilde{g}([\mathbf{h}_{[i,:]} \mathbf{W} \| \mathbf{h}_{[\varphi(i),:]} \mathbf{W}]) > \tilde{g}([\mathbf{h}_{[i,:]} \mathbf{W} \| \mathbf{h}_{[j,:]} \mathbf{W}]) = 0. \quad (40)$$

If we concatenate the two input vectors, and define the scoring function e of the graph attention layer (29) as a function of the concatenated vector $[\mathbf{h}_{[i,:]} \mathbf{W} \| \mathbf{h}_{[j,:]} \mathbf{W}]$, from the universal approximation theorem [37], e can approximate \tilde{g} for any compact subset of \mathbb{R}^{2D_k} .

Thus, for any sufficiently small ϵ (any $0 < \epsilon < \frac{1}{2}$) there exist parameters \mathbf{W}_{att} and \mathbf{v}_{att} such that for every node $i \in \mathcal{V}$ and every $j \neq \varphi(i)$:

$$\begin{aligned} e(\mathbf{h}_{[i,:]} \mathbf{W}, \mathbf{h}_{[\varphi(i),:]} \mathbf{W}) &> 1 - \epsilon \\ &> 0 + \epsilon \\ &> e(\mathbf{h}_{[i,:]} \mathbf{W}, \mathbf{h}_{[j,:]} \mathbf{W}) \end{aligned} \quad (41)$$

and due to the increasing monotonicity of softmax:

$$\alpha_{i,\varphi(i)} > \alpha_{i,j}. \quad (42)$$

C. Proof of Theorem 3

The expression for the attention coefficient, as defined in Eq. (16), can be reformulated as follows:

$$e_{ij}^A = \sum_{k=1}^{F_A} u_{ij}^k, \quad (43)$$

where

$$u_{ij}^k = |\phi(\mathbf{x}_{[i,:]} [\mathbf{W}_A]_k) - \phi(\mathbf{x}_{[j,:]} [\mathbf{W}_A]_k)| \cdot [\mathbf{v}_A]_k. \quad (44)$$

Here, the notation $[\cdot]_k$ represents the k -th column vector or the k -th element of a matrix or vector.

²The function \tilde{g} is a function that we define for the ease of proof, because the universal approximation theorem is defined for continuous functions, and we only need the scoring function of the graph attention layer e to approximate the mapping φ in a finite set of points. So, we need the attention function e to approximate g (from Equation 8) in some specific points. But, since g is not continuous, we define \tilde{g} and use the universal approximation theorem for \tilde{g} . Since e approximates \tilde{g} , e also approximates g in our specific points, as a special case. We only require that \tilde{g} will be identical to g in specific N^2 points $\{[\mathbf{h}_{[i,:]} \| \mathbf{h}_{[j,:]}] \mid i, j \in [N]\}$. For the rest of the input space, we don't have any requirement on the value of \tilde{g} , except for maintaining the continuity of \tilde{g} . There exist infinitely many such possible \tilde{g} for every given set of keys, queries and a mapping φ , but the concrete functions are not needed for the proof.

Based on the decomposition of the summation in Eq. 43, we focus on the k -th term, denoted as u_{ij}^k . Let $c_j^k := \phi(\mathbf{x}_{[j,:]}[\mathbf{W}_A]k)$, and then sort $c_j^k, \forall j \in \mathcal{N}_i^C$ in ascending order to obtain the corresponding indices of the node sorting, denoted as $\{j_{min}, \dots, j_{l_1}, j, j_{r_1}, \dots, j_{max}\}$. Assuming the scalar $[\mathbf{v}_A]k$ is positive, the maximum value of u_{ij}^k can be obtained as follows:

$$\max \left\{ |c_i^k - c_{j_{max}}^k|, |c_i^k - c_{j_{min}}^k| \right\}, j \in \mathcal{N}_i^C \quad (45)$$

Conversely, if the scalar $[\mathbf{v}_A]k$ is negative, the maximum value of u_{ij}^k is given by:

$$\max \left\{ \left| c_i^k - c_{j_{l_1}}^k \right|, \left| c_i^k - c_{j_{r_1}}^k \right| \right\}, j \in \mathcal{N}_i^C \quad (46)$$

It is evident that the selection of the maximum value of u_{ij}^k is not fixed but rather depends on \mathcal{N}^C and $[\mathbf{v}_A]k$. Thus, u_{ij}^k , as the attention coefficient in the summation of e_{ij}^k for the k -th term, exhibits a dynamic attention property.

Similar conclusions can be drawn for the remaining $F_A - 1$ terms, wherein the difference arises due to the varying orders of $c_j^k, \forall j \in \mathcal{N}_i^C$ determined by the specific values of $[\mathbf{W}_A]k$ and $[\mathbf{v}_A]k$, which further ensures the dynamic attention property.

D. Proof of Theorem 4

The gradient with respect to \mathbf{S}' at \mathbf{S} is $\frac{\partial \mathcal{L}}{\partial \mathbf{S}'} \Big|_{\mathbf{S}'=\mathbf{S}} = 2c\mathbf{L}\mathbf{S}$. Hence, one-step gradient descent for the graph signal denoising problem (30) can be described as:

$$\mathbf{S}' \leftarrow \mathbf{S} - b \frac{\partial \mathcal{L}}{\partial \mathbf{S}'} \Big|_{\mathbf{S}'=\mathbf{S}} = \mathbf{S} - 2bc\mathbf{L}\mathbf{S} = (1 - 2bc)\mathbf{S} + 2bc\hat{\mathbf{A}}\mathbf{S}. \quad (47)$$

When stepsize $b = \frac{1}{2c}$ and $\mathbf{S} = \mathbf{H}^{(k-1)}$, we have $\mathbf{S}' \leftarrow \hat{\mathbf{A}}\mathbf{H}^{(k-1)}$, which is the same as the aggregation operation of GCN.

E. Proof of Theorem 5

The gradient of Eq. (34) with respect to \mathbf{S}' focusing on a node i can be written as:

$$\frac{\partial \mathcal{L}}{\partial \mathbf{S}'_{[i,:]}} = 2(\mathbf{s}_{[i,:]} - \mathbf{s}_{[i,:]}) + \sum_{j \in \mathcal{N}(i)} (c_i + c_j) (\mathbf{s}'_{[i,:]} - \mathbf{s}'_{[j,:]}), \quad (48)$$

where c_j in the second term appears since i is also in the neighbor of j . Then, the gradient at \mathbf{S} is

$$\frac{\partial \mathcal{L}}{\partial \mathbf{S}'_{[i,:]}} \Big|_{\mathbf{S}'=\mathbf{S}} = \sum_{j \in \mathcal{N}(i)} (c_i + c_j) (\mathbf{s}_{[i,:]} - \mathbf{s}_{[j,:]}). \quad (49)$$

Thus, one step of gradient descent starting from \mathbf{S} with stepsize b_i is as follows:

$$\begin{aligned} \mathbf{s}'_{[i,:]} &\leftarrow \mathbf{s}_{[i,:]} - b_i \frac{\partial \mathcal{L}}{\partial \mathbf{S}'_{[i,:]}} \Big|_{\mathbf{S}'=\mathbf{S}} \\ &= \left(1 - b_i \sum_{j \in \mathcal{N}(i)} (c_i + c_j)\right) \mathbf{s}_i + \sum_{j \in \mathcal{N}(i)} b_i (c_i + c_j) \mathbf{s}_j \end{aligned} \quad (50)$$

Given $b_i = 1 / \sum_{j \in \mathcal{N}(i)} (c_i + c_j)$, Eq. (51) can be rewritten as

$$\mathbf{s}'_{[i,:]} \leftarrow \sum_{j \in \mathcal{N}(i)} b_i (c_i + c_j) \mathbf{s}_j, \quad (52)$$

which completes the proof.

F. Proof of Theorem 6

The complexity analysis of the k -th graph convolutional layer can be segmented into two components: Eq. (4) and Eq. (5).

First, we consider the operation described in Eq. (4), which entails a matrix product involving a sparse adjacency matrix and a dense representation matrix. Specifically, the i -th row of $\bar{\mathbf{H}}^{(k)}$ can be expressed as follows:

$$\bar{\mathbf{h}}_{[i,:]} = \hat{\mathbf{a}}_{[i,:]} \mathbf{H}^{(k-1)} = \sum_{j=1}^N \hat{a}_{ij} \mathbf{h}_{[j,:]}^{(k-1)} = \sum_{j \in \mathcal{N}_i} \hat{a}_{ij} \mathbf{h}_{[j,:]}^{(k-1)}. \quad (53)$$

Here, the computation of $\bar{\mathbf{h}}_{[i,:]}$ demands $O(|\mathcal{N}_i|D_{k-1})$ in terms of time complexity. Given that $2|E| = \sum_{i=1}^N |\mathcal{N}_i|$, the overall time complexity for Eq. (4) becomes $O(|E|D_{k-1})$.

Secondly, for the matrix multiplication between two dense matrices, as seen in Eq. (5), the well-known time complexity is $O(ND_{k-1}D_k)$.

In summary, the time complexity of the k -th graph convolutional layer can be succinctly expressed as $O(ND_{k-1}D_k + |E|D_{k-1})$.

G. Proof of Theorem 7

The proof of Theorem 7 comprises three distinct parts, each pertaining to the time complexity analysis of ALM-I, ALM-II, and the k -th graph attention layer within the Multi-Graph Attention Layer (MGAL). We shall address them individually:

- The operations involved in ALM-I, as described by Eq. (10), Eq. (14), and Eq. (15), all require $O(N)$ time complexity.
- The primary computational complexity within ALM-II arises from the calculation of attention coefficients, as articulated in Eq. (16).
 - Firstly, we compute $\mathbf{x}_{[i,:]} \mathbf{W}_A$ for every $i \in [N]$, which necessitates $O(NNF_A)$;

- Subsequently, for each edge (i, j) , we compute $|\phi(\mathbf{x}_{[i,:]} \mathbf{W}_A) - \phi(\mathbf{x}_{[j,:]} \mathbf{W}_A)|$ using the precomputed $\mathbf{x}_{[i,:]} \mathbf{W}_A$ and $\mathbf{x}_{[j,:]} \mathbf{W}_A$, incurring a time complexity of $O(|E^C|F_A)$;
- Finally, computing the results of the linear layer \mathbf{v}_A adds an additional $O(|E^C|F_A)$.

In summary, the time complexity of ALM-I amounts to $O(NNF_A + |E^C|F_A)$.

- The computational complexity of the k-th graph attention layer within MGAL can be broken down into several components:
 - Initially, we compute Eq. (22) for every $i \in [N]$, demanding $O(ND_{k-1}D_k)$;
 - Subsequently, we calculate $\hat{\mathbf{h}}_{[i,:]}^{(k-1)} \mathbf{W}_{att}^{(k-1)}$ for every $i \in [N]$ using the precomputed $\hat{\mathbf{h}}_{[i,:]}^{(k-1)}$, which incurs a time complexity of $O(ND_k F_{att})$;
 - Further, computing the results of the linear layer \mathbf{v}_{att}^{k-1} takes $O(|E^F|F_A)$;
 - Finally, we compute Eq.(24) for every $i \in [N]$, requiring $O(|E^F|D_k)$.

Consequently, the time complexity for the k-th graph attention layer within MGAL is given by $O(ND_k F_{att} + ND_{k-1}D_k + |E^F|F_{att} + |E^F|D_k)$.

By systematically analyzing each component, we have established the respective time complexities for ALM-I, ALM-II, and the k-th graph attention layer within MGAL as outlined above.

REFERENCES

- [1] T. N. Kipf and M. Welling, “Semi-Supervised Classification with Graph Convolutional Networks,” in *International Conference on Learning Representations (ICLR)*, 2017.
- [2] W. Hamilton, Z. Ying, and J. Leskovec, “Inductive Representation Learning on Large Graphs,” in *Advances in neural information processing systems (NIPS)*, 2017, pp. 1024–1034.
- [3] P. Veličković, G. Cucurull, A. Casanova, A. Romero, P. Lio, and Y. Bengio, “Graph Attention Networks,” 2017.
- [4] K. Xu, W. Hu, J. Leskovec, and S. Jegelka, “How Powerful Are Graph Neural Networks,” 2019.
- [5] A. Ortega, P. Frossard, J. Kovačević, J. M. Moura, and P. Vandergheynst, “Graph Signal Processing: Overview, Challenges, and Applications,” *Proceedings of the IEEE*, vol. 106, no. 5, pp. 808–828, 2018.
- [6] F. Gama, A. G. Marques, G. Leus, and A. Ribeiro, “Convolutional Neural Network Architectures for Signals Supported on Graphs,” *IEEE Transactions on Signal Processing*, vol. 67, no. 4, pp. 1034–1049, 2018.
- [7] K. C. Dzmitry Bahdanau and Y. Bengio, “Neural Machine Translation by Jointly Learning to Align and Translate,” *International Conference on Learning Representations*, 2015.
- [8] A. W. Yu, D. Dohan, M.-T. Luong, R. Zhao, K. Chen, M. Norouzi, and Q. V. Le, “QANet: Combining Local Convolution with Global Self-Attention for Reading Comprehension,” in *International Conference on Learning Representations*, 2018.
- [9] A. Vaswani, N. Shazeer, N. Parmar, J. Uszkoreit, L. Jones, A. N. Gomez, Ł. Kaiser, and I. Polosukhin, “Attention Is All You Need,” *Advances in neural information processing systems*, vol. 30, 2017.
- [10] N. Patwari, A. O. Hero, M. Perkins, N. S. Correal, and R. J. O’Dea, “Relative Location Estimation in Wireless Sensor Networks,” *IEEE Transactions on Signal Processing*, vol. 51, no. 8, pp. 2137–2148, Aug 2003.
- [11] F. Yin, C. Fritsche, F. Gustafsson, and A. M. Zoubir, “EM- and JMAP-ML Based Joint Estimation Algorithms for Robust Wireless Geolocation in Mixed LOS/NLOS Environments,” *IEEE Transactions on Signal Processing*, vol. 62, no. 1, pp. 168–182, 2013.
- [12] A. Simonetto and G. Leus, “Distributed Maximum Likelihood Sensor Network Localization,” *IEEE Transactions on Signal Processing*, vol. 62, no. 6, pp. 1424–1437, 2014.
- [13] F. Yin, C. Fritsche, F. Gustafsson, and A. M. Zoubir, “TOA-Based Robust Wireless Geolocation and Cramér-Rao Lower Bound Analysis in Harsh LOS/NLOS Environments,” *IEEE transactions on signal processing*, vol. 61, no. 9, pp. 2243–2255, 2013.
- [14] H. Wymeersch, J. Lien, and M. Z. Win, “Cooperative Localization in Wireless Networks,” *Proceedings of the IEEE*, vol. 97, no. 2, pp. 427–450, 2009.
- [15] J. Costa, N. Patwari, and A. Hero, “Distributed Weighted-Multidimensional Scaling for Node Localization in Sensor Networks,” *ACM Transactions on Sensor Networks*, vol. 2, no. 1, pp. 39–64, 2006.
- [16] P. Biswas, T. Lian, T. Wang, and Y. Ye, “Semidefinite Programming Based Algorithms for Sensor Network Localization,” *ACM Transactions on Sensor Networks*, vol. 2, no. 2, pp. 188–220, May 2006.
- [17] P. Tseng, “Second-Order Cone Programming Relaxation of Sensor Network Localization,” *SIAM Journal on Optimization*, vol. 18, no. 1, pp. 156–185, 2007.
- [18] A. Ihler, J. W. Fisher, R. L. Moses, and A. S. Willsky, “Non-parametric Belief Propagation for Self-Localization of Sensor Networks,” in *IEEE Journal on Selected Areas in Communications*, 2005.
- [19] D. Jin, F. Yin, C. Fritsche, F. Gustafsson, and A. M. Zoubir, “Bayesian cooperative localization using received signal strength with unknown path loss exponent: Message passing approaches,” *IEEE Transactions on Signal Processing*, vol. 68, pp. 1120–1135, 2020.
- [20] S. Marano, W. M. Gifford, H. Wymeersch, and M. Z. Win, “NLOS Identification and Mitigation for Localization Based on UWB Experimental Data,” *IEEE Journal on Selected Areas in Communications*, vol. 28, no. 7, pp. 1026–1035, Sep. 2010.
- [21] F. Yin, C. Fritsche, D. Jin, F. Gustafsson, and A. M. Zoubir, “Cooperative Localization in WSNs Using Gaussian Mixture Modeling: Distributed ECM Algorithms,” *IEEE Transactions on Signal Processing*, vol. 63, no. 6, pp. 1448–1463, 2015.
- [22] H. Chen, G. Wang, Z. Wang, H. C. So, and H. V. Poor, “Non-Line-of-Sight Node Localization Based on Semi-Definite Programming in Wireless Sensor Networks,” *IEEE Transactions on Wireless Communications*, vol. 11, no. 1, pp. 108–116, 2012.
- [23] D. Jin, F. Yin, M. Fauß, M. Muma, and A. M. Zoubir, “Exploiting Sparsity for Robust Sensor Network Localization in Mixed LOS/NLOS Environments,” in *IEEE International Conference on Acoustics, Speech and Signal Processing (ICASSP)*, 2020, pp. 5915–5915.
- [24] D. Jin, F. Yin, A. M. Zoubir, and H. C. So, “Exploiting Sparsity of Ranging Biases for NLOS Mitigation,” *IEEE Transactions on Signal Processing*, vol. 69, pp. 3782–3795, 2021.

- [25] W. Yan, D. Jin, Z. Lin, and F. Yin, “Graph Neural Network for Large-Scale Network Localization,” in *ICASSP 2021-2021 IEEE International Conference on Acoustics, Speech and Signal Processing (ICASSP)*. IEEE, 2021, pp. 5250–5254.
- [26] F. Yin, Z. Lin, Q. Kong, Y. Xu, D. Li, S. Theodoridis, and S. R. Cui, “FedLoc: Federated Learning Framework for Data-Driven Cooperative Localization and Location Data Processing,” *IEEE Open Journal of Signal Processing*, vol. 1, pp. 187–215, 2020.
- [27] R. Zekavat and R. M. Buehrer, *Handbook of Position Location: Theory, Practice and Advances*. John Wiley & Sons, 2011, vol. 27.
- [28] F. Wu, T. Zhang, A. H. d. Souza Jr, C. Fifty, T. Yu, and K. Q. Weinberger, “Simplifying Graph Convolutional Networks,” in *International Conference on Learning Representations (ICLR)*, 2019.
- [29] D. Svozil, V. Kvasnicka, and J. Pospichal, “Introduction to Multi-layer Feed-forward Neural Networks,” *Chemometrics and Intelligent Laboratory Systems*, vol. 39, no. 1, pp. 43–62, 1997.
- [30] P. Ramachandran, B. Zoph, and Q. V. Le, “Searching for Activation Functions,” in *International Conference on Learning Representations (ICLR)*, 2018.
- [31] L. Bottou, “Large-Scale Machine Learning with Stochastic Gradient Descent,” in *Proceedings of 19th International Conference on Computational Statistics*. Springer, 2010, pp. 177–186.
- [32] D. P. Kingma and J. Ba, “Adam: A Method for Stochastic Optimization,” in *International Conference on Learning Representations (ICLR)*, 2014.
- [33] A. Sandryhaila and J. M. Moura, “Discrete Signal Processing on Graphs: Frequency Analysis,” *IEEE Transactions on Signal Processing*, vol. 62, no. 12, pp. 3042–3054, 2014.
- [34] F. Gama, E. Isufi, G. Leus, and A. Ribeiro, “Graphs, Convolutions, and Neural Networks: From Graph Filters to Graph Neural Networks,” *IEEE Signal Processing Magazine*, vol. 37, no. 6, pp. 128–138, 2020.
- [35] U. A. Brody, S. and E. Y., “How Attentive Are Graph Attention Networks?” 2022.
- [36] X. Wu, A. Ajourlou, Z. Wu, and A. Jadbabaie, “Demystifying oversmoothing in attention-based graph neural networks,” *arXiv preprint arXiv:2305.16102*, 2023.
- [37] K. Hornik, “Approximation capabilities of multilayer feedforward networks,” *Neural networks*, vol. 4, no. 2, pp. 251–257, 1991.
- [38] Y. Ma, L. Xiaorui, Z. Tong, L. Yozen, T. Jiliang, and S. Neil, “A Unified View on Graph Neural Networks as Graph Signal Denoising,” in *Proceedings of the 30th ACM International Conference on Information and Knowledge Management*, 2021, pp. 1202–1211.
- [39] J. Bruna, W. Zaremba, A. Szlam, and Y. LeCun, “Spectral networks and deep locally connected networks on graphs,” in *ICLR*, 2014.
- [40] M. Defferrard, X. Bresson, and P. Vandergheynst, “Convolutional neural networks on graphs with fast localized spectral filtering,” *NIPS*, vol. 29, 2016.